

THE EVIDENCE FOR THE OBSERVATION OF $0\nu\beta\beta$ DECAY: THE IDENTIFICATION OF $0\nu\beta\beta$ EVENTS FROM THE FULL SPECTRA

H. V. KLAPDOR-KLEINGROTHAUS* and I. V. KRIVOSHEINA†

Max-Planck-Institut für Kernphysik, P. O. 103980, D-69029 Heidelberg, Germany

**h.klapdor@mpi-hd.mpg.de*

†irina.krivosheina@mpi-hd.mpg.de

Received 8 March 2006

In this brief review, a description of the observed evidence for neutrinoless double beta^{3–5} in the ⁷⁶Ge experiment in Gran Sasso (Heidelberg–Moscow experiment) which has been operated with 11 kg enriched ⁷⁶Ge detectors in the period 1990–2003, is provided. Two different methods of pulse shape analysis have been used to select potential $0\nu\beta\beta$ events from the γ background of the measured spectrum — a selection by a neuronal net approach,^{3,4,16} and a selection by a new method comparing measured pulses with a library of pulse shapes of point-like events calculated from simulation of the electric field distribution in the detectors (see Refs. 6–8 and 37). The latter method also allows spatial localization of measured events. Both methods lead to *selections of events at $Q_{\beta\beta}$ with almost no γ -background*. The observed line at $Q_{\beta\beta}$ is identified as a $0\nu\beta\beta$ signal. It has a confidence level of more than 6σ .

Keywords: Neutrino mass and mixing; Majorana neutrino; beta-decay; double beta decay; Heidelberg–Moscow experiment; high purity Ge detectors.

PACS Nos.: 14.60.Pq, 23.40.-s, 29.40.-n, 95.55.Vj

1. Introduction

Nuclear double beta decay provides an extraordinarily broad potential to search for beyond standard model physics.^{1,2} Its occurrence has enormous consequences: it means that *total lepton number is not conserved*. Second, it proves that the *neutrino is a Majorana particle*. Furthermore, it can provide, *under some assumptions*, an absolute scale of the neutrino mass, and yields sharp restrictions for SUSY models, leptoquarks, compositeness, left–right symmetric models, test of special relativity and equivalence principle in the neutrino sector, and others.^{1,2}

Among the many existing efforts in search for this process, for 13 years now the Heidelberg–Moscow experiment¹³ which operated 11 kg of enriched high-purity ⁷⁶Ge detectors (the first ones ever produced) in the period 1990–2003 in the GRAN

*Spokesman of Heidelberg–Moscow, GENIUS-TF and HDMS Collaborations.

†On leave from Radiophysical-Research Institute, Nishnii-Novgorod, Russia.

SASSO underground laboratory is by far the most sensitive double beta experiment. Since 2001, the experiment was operated *only* by Heidelberg group, which also performed the analysis of the experiment from its very beginning.

The first and up to now only evidence for $0\nu\beta\beta$ decay has been reported from this experiment.^{2–5,9–12} In the period 1995–2003 which delivered the main set of data, the time structure of all events have been registered. These pulse shapes have been used earlier in the search for $0\nu\beta\beta$ pulses among others by a neuronal net.^{3,4} Since then, an independent *new method* has been developed (see also Ref. 17) which is *complementary* and of *similar selectivity* as the neuronal net used earlier. It confirms independently the existence of a signal at $Q_{\beta\beta}$.^a

The new method is based on building pulse shape libraries for search of sharply localized events in the detector as function of location, for the four main detectors of the Heidelberg–Moscow experiment. Starting from the Monte Carlo calculated time history and spatial distribution of $0\nu\beta\beta$ events we have for this purpose for the *first time* calculated the pulse shapes to be expected microscopically (see also Refs. 6–8 and 17). The library is “calibrated” by γ -source measurements with a collimator which were performed in the period July to September 2004 in the Gran Sasso underground laboratory and measured shapes of pulses as function of radius and height of the detectors. It was found that it is possible to select very efficiently small size (low multiplicity) events, such as $0\nu\beta\beta$ events, by rejecting the background of large-size (high multiplicity) gamma events. The method also allows to determine their localization in the detector.

For a proof of observation of neutrinoless double beta decay, a method is required, which fulfills the following criteria: (1) select $0\nu\beta\beta$ events at $Q_{\beta\beta}$, (2) reduce strongly surrounding γ events.

In this review we show that our two methods: neuronal and new method, fulfill these criteria, and lead to fully consistent results. We present here a *final detailed discussion* of the results of the analysis of the Heidelberg–Moscow experiment for the measuring period 1995–2003. We show that we have now *two projections of events with almost no background*, which both prove the existence of a line at $Q_{\beta\beta}$ which we identify as $0\nu\beta\beta$ signal. This signal seen in the pulse shape analyzed spectra has a confidence level of $\sim 6\sigma$.

2. Structure of Double Beta Events and the Corresponding Pulse Shapes

2.1. Monte Carlo simulated tracks and the pulse shapes

The half-life for the neutrinoless decay mode is given by^{30,31} $[T_{1/2}^{0\nu}(0_i^+ \rightarrow 0_f^+)]^{-1} = C_{mm} \frac{\langle m \rangle^2}{m_e^2} + C_{\eta\eta} \langle \eta \rangle^2 + C_{\lambda\lambda} \langle \lambda \rangle^2 + C_{m\eta} \langle \eta \rangle \frac{\langle m \rangle}{m_e} + C_{m\lambda} \langle \lambda \rangle \frac{\langle m \rangle}{m_e} + C_{\eta\lambda} \langle \eta \rangle \langle \lambda \rangle$, $\langle m \rangle =$

^aAn independent analysis of the data taken until 2000 has been performed in Ref. 36. Another analysis of part of the data has been shown to be wrong in Ref. 3, p. 201 and Ref. 4, pp. 382 and 385. Some earlier criticism has already been ruled out in Refs. 9 and 39, i.e. it was already history before the higher statistics data were presented in Refs. 3 and 4.

$|m_{ee}^{(1)}| + e^{i\phi_2}|m_{ee}^{(2)}| + e^{i\phi_3}|m_{ee}^{(3)}|$, where $m_{ee}^{(i)} \equiv |m_{ee}^{(i)}|\exp(i\phi_i)$ ($i = 1, 2, 3$) are the contributions to the effective mass $\langle m \rangle$ from individual mass eigenstates, with ϕ_i denoting relative Majorana phases connected with CP violation, and $C_{mm}, C_{\eta\eta}, \dots$ denote nuclear matrix elements squared. Ignoring contributions from right-handed weak currents on the right-hand side of the above equation, only the first term remains.

The tracks of $0\nu\beta\beta$ events in a Ge detector (see Fig. 1, and Fig. 6 of Ref. 6) and their resulting electrical pulses depend in principle on the spectral-angular correlations of the emitted electrons. These correlations have been calculated recently for the case of ^{76}Ge .^{6–8}

The *sizes* of the Monte Carlo simulated events have been calculated and it has been shown that $0\nu\beta\beta$ tracks *can be well separated* in size from normal γ -lines, but are similar to double escape (DE) lines such as the 1592 keV DE line of the 2614 keV transition (for details see Refs. 6–8). Also part of the Compton events in the range around $Q_{\beta\beta}$ from the 2614 keV of ^{228}Th line occurring as background in the measured spectra (see Refs. 3 and 4) can be separated by size from $\beta\beta$ events. It is important to note that the spectrum of the Compton events is *flat* in this energy range.^{4,28} Calculation of the shapes of the *electrical pulses* in a Ge detector corresponding to the calculated tracks, i.e. taking the spatial distribution of energy fully into account shows,¹⁷ that the *limited position resolution* of the detector *washes out the differences* still seen in the tracks, to some extent. So neither the *differences in size* of individual $0\nu\beta\beta$ events nor the differences seen *in size* still for $\beta\beta$ events of different mechanisms (mass term or right-handed current parameters λ, η), are seen anymore for the majority of $\beta\beta$ pulses ($\sim 90\%$) which have shapes smaller than 2(0.5) mm (linear and weighted size, respectively).¹⁷

The situation becomes different for the rare but existing large $0\nu\beta\beta$ pulses (weighted sizes > 1 mm). Here the “degeneracy” of shape of individual pulses and partly from different mechanisms is *lifted* (for details see Ref. 17).

2.2. Zero range library

Since our Monte Carlo calculations (see Refs. 6–8) show, that most $\beta\beta$ -events have a small size, a library of pulses has been built up for pulses, in which *all energy* of the event is assumed to be *deposited in one point* in the detector (*zero range approximation*). This is found to be a good approximation for $\sim 90\%$ of the $\beta\beta$ events (see Ref. 17). An example is shown in Fig. 1 where a relatively large size microscopically calculated (see Sec. 2.1) $0\nu\beta\beta$ event pulse shape (here the final pulse is a sum of typically a few hundred subpulses), is compared with the result assuming a point-like event.

This observation has been exploited for the analysis of the double beta experiment using ^{76}Ge . A library of zero range pulse shapes has been built up for the four detectors which measured the pulse shapes of events in the period 1995–2003, throughout the detector volume. Pulses measured in the Heidelberg–Moscow

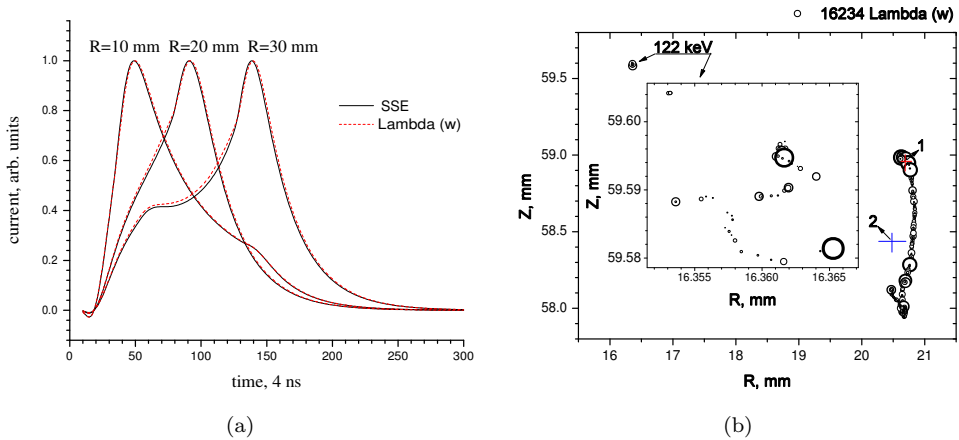


Fig. 1. (a) Comparison of a Monte Carlo simulated $0\nu\beta\beta$ pulse (No. 16234) (produced by the right-handed current term λ (see Eq. (1)) (red dotted line) and a calculated zero range single site event of same energy with a starting point at $R = 10, 20, 30$ mm and $Z = 5.57$ mm (black line). (b) The calculated track of this event (parameters: weighted size (w) = 0.5 mm, linear size (l) = 4.65 mm). In the extra window, the detailed structure of the above sub-event is shown. Red (1) and blue (2) crosses indicate different choices for the localization of the event in R . (1) sets it equal to the starting point of the $\beta\beta$ event, (2) sets it equal to the center of gravity (concerning the energy distribution) of the event.

experiment will later in this paper be compared to pulses of this calculated library. The method of calculation follows the standard procedure and has been described in Ref. 17. Such pulse shape calculations are a very complex task and can be done only by doing various approximations (see, e.g. Refs. 21–27). So until now e.g. no theoretically-based formula exists which describes the field dependence of the drift velocity of the charge carriers. Several parameters have been used as fit parameter in the approach used here. For details see Ref. 17.

2.3. Test of the library by source measurements

Optimization of the library calculated as described in Sec. 2.2 and Ref. 17, was done iteratively in order to reach simultaneously the best possible localization of events along the detector volume for a given placement of the collimator, as well as to reach the best suppression of the 1620 keV line which is mainly consisting of higher multiplicity (larger size) events similar to the full energy peak at 2614 keV, with respect to the double escape γ -line of the 2614 keV transition, which is known (see, e.g. Refs. 6–8 and 20) to consist of very sharply localized events at 1592 keV. This optimization was done mostly by slightly varying the impurity density (not in the calculations with the realistic impurity distribution, see below) and the scaling of the hole mobility (for details we refer to Ref. 17).

Figure 2 shows an example of the result of the analysis of source measurements for the 238 keV γ -line from ^{228}Th . These low-energy γ -events should be very well localized in the detector (single site events — SSE).

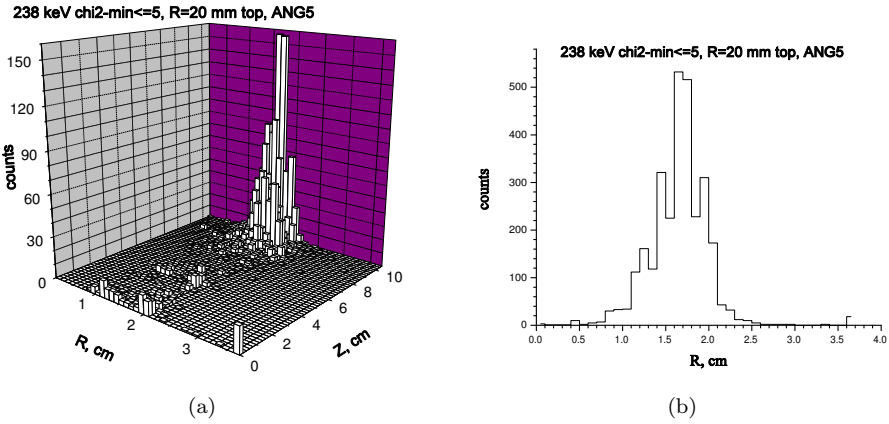


Fig. 2. Upper part: three-dimensional localization of the 238 keV line from the data of calibration of detector 5 of the Heidelberg–Moscow $\beta\beta$ experiment for location of the radioactive source at $R = 20$ mm (a), by the zero range library calculated as described in Sec. 2.2 ($\chi^2 < 5$). (b) Radial localization, corresponding to (a) of the figure.

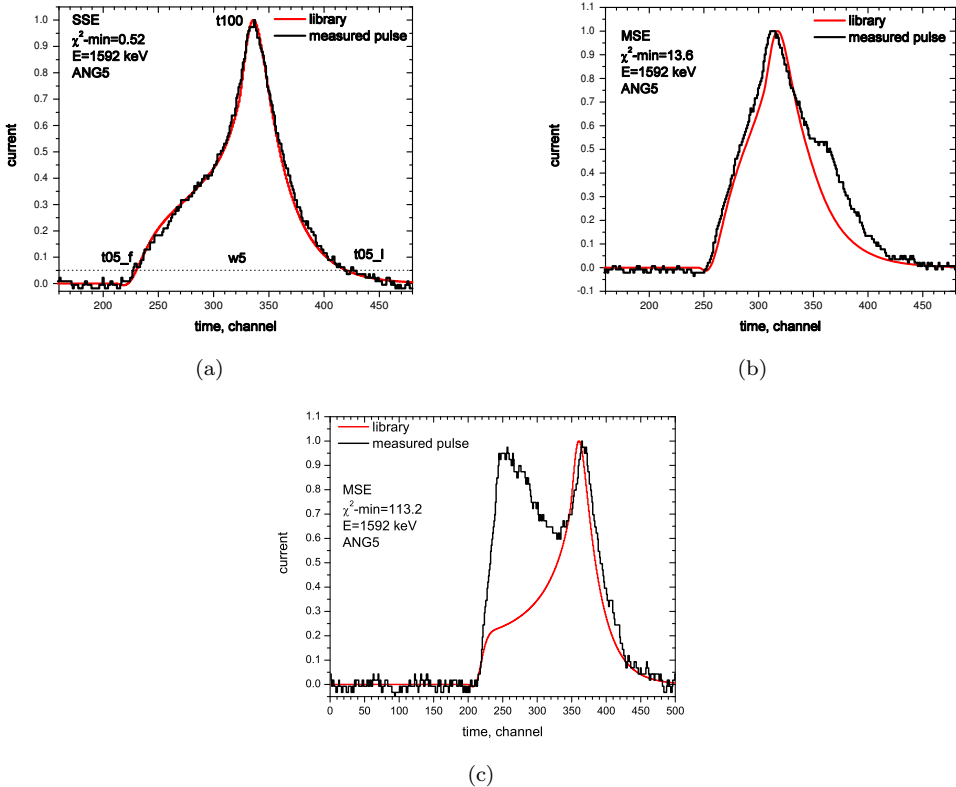


Fig. 3. Result of fitting experimental pulse shapes (black) with the library shapes (red) for events of the double escape line at 1592 keV of the 2614 keV transition from a ^{228}Th source. (a) represents a single site event (SSE), (b) a multiple site event (MSE) event. A more drastic MSE event is shown in (c).

Finally we show in Fig. 3, typical fits of measured γ -pulses (data from the calibration measurements for the Heidelberg–Moscow experiment (here of the 1592 keV double escape γ -line of the 2614 keV transition from a ^{228}Th source), by the zero range library. This line is known to consist dominantly of single site events (see Refs. 3, 4, 6–8 and 20). Figure 3(a) is classified as a single site event (SSE), the other two are clearly identified as multiple site events.

3. Application of the Zero Range Pulse Shape Library to the Double Beta Decay Data of the Heidelberg–Moscow Experiment and Comparison to the Neuronal Net Results

We apply now the calculated library for the zero-range approximation described in Secs. 2.2 and 2.3 and Ref. 17 to the events from the spectrum measured with detectors 2, 3, 4, 5 in the Heidelberg–Moscow experiment in the period 1995–2003 (see Refs. 3 and 4). For these detectors, which have a total mass of 10 kg, the pulse shapes had been measured with a 250 MHz flash ADC. We discuss the results in connection with those obtained^{3,4} by pulse shape analysis using a neuronal net.

Accepting only measured pulses which are fitted by a library event with small χ^2 ,^b ($\chi^2 < 0.4, 0.4, 0.7, 0.35$ for detectors 2, 3, 4, 5, respectively), the result is a *very* drastic reduction of *any* γ -lines in the measured spectrum (Fig. 4). A similar reduction we get from the selection with the neuronal net (Fig. 5) when selecting a subclass (NN) as discussed below.

Note that in particular multiple site events (which are typically dominating a normal γ -line) *are suppressed by 100%*. An example is the line at 2505.7 keV, seen in the full spectrum (see Fig. 16 of Ref. 4 or Fig. 3 (right) of Ref. 3). It is expected, as sum line of the 1173.2 and 1332.5 keV ^{60}Co lines, to consist of practically 100% of MSE. Figure 6 shows that the neuronal net (see Ref. 4) classified this line to practically fully consisting of multiple site events. The suppression is (see Fig. 4) 100% for the MSE events. While for the “global” neuronal net cut (more precisely HNR+NN, see below) the γ -lines around $Q_{\beta\beta}$ were far from completely suppressed (see Fig. 31 in Ref. 4), *we now obtain an almost complete suppression* when applying the low- χ^2 cut, and also when applying the neuronal subset (NN) selection. In particular practically *no MSE* events are observed in these selections (see also Table 1). This is demonstrated in Fig. 7.

We show in Fig. 7 the spectrum obtained by these low- χ^2 cuts with the zero range pulse shape method, for the full detector volumes *and* those obtained when

^bWe define chi-squared here as a sum of squared deviations between the time structures of measured pulse and library pulse: $\chi^2 = \sum_{n=t05-f}^{t05-l} \frac{(i_{\text{exp}}^n - i_{\text{lib}}^n)^2}{w5} \cdot 10^3$. Here i_{exp}^n and i_{lib}^n are the (normalized) experimental and library currents for the (time) channel n (one time step is 4 ns per channel of the flash-ADC sampling frequency of 250 MHz). $w5$ is the width at the 5% level of the amplitude (see Fig. 3). χ_{min}^2 gives the degree of agreement of a measured pulse with the library pulse “closest” in shape (time structure) to the measured pulse. For a detailed description see Ref. 37.

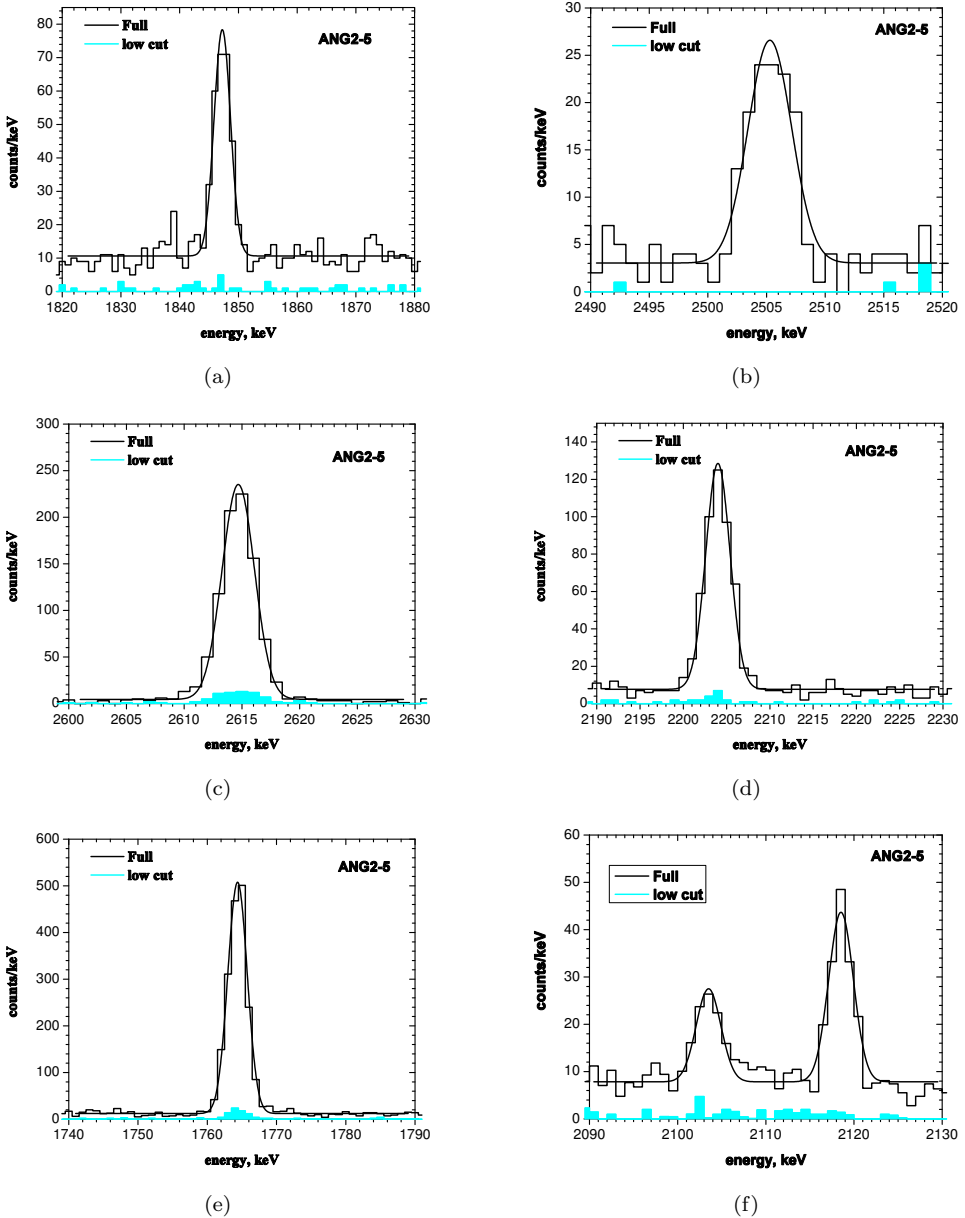


Fig. 4. Lines from the full spectrum measured Nov. 1995–May 2003 (see also Figs. 15 and 16 of Ref. 4, and Fig. 3 of Ref. 3 — note that in the captions of these figures it should read “from Nov. 1995 to May 2003”) and the pulse shape selected spectrum on the basis of the zero range library with small χ^2 cut (see text), for detectors 2, 3, 4, 5 in the energy regions of some strong background lines. The γ -lines are drastically reduced. Even some fine details of the composition of γ -lines are “seen” by this selection of small site events. E.g. the 2505.7 keV line (see Refs. 3 and 4) originating from summation of the subsequent 1173.2 and 1332.5 keV γ -lines from ^{60}Co naturally expected to be a *multiple site event* is *erased to 100%*, as is also the case when applying the neuronal net (see Fig. 5).

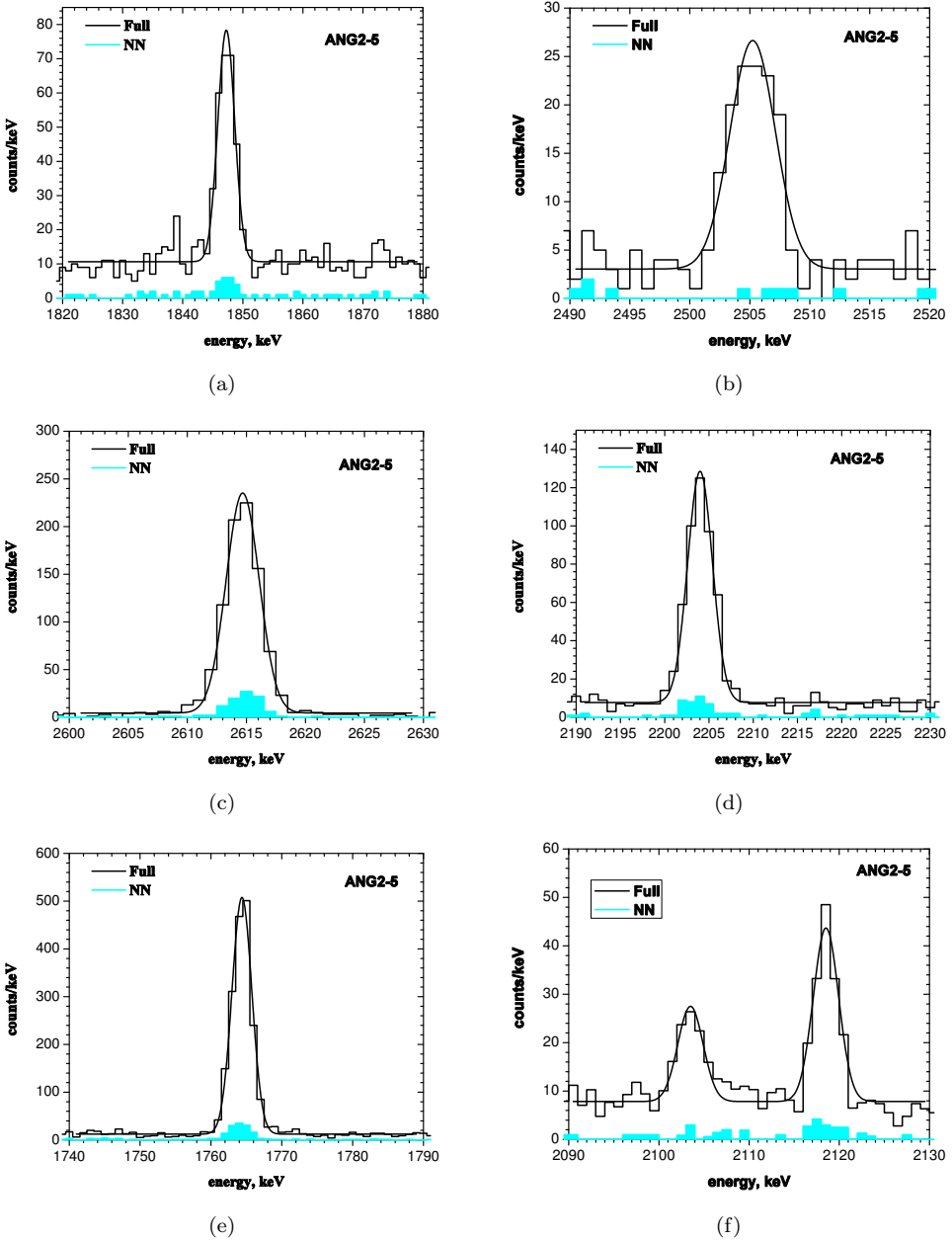


Fig. 5. Lines from the neuronal net (NN) pulse shape selected spectrum measured 1995–2003 (Fig. 9 and 33 respectively of Refs. 3 and 4) for detectors 2, 3, 4, 5 in the energy regions of some strong background lines. Even some fine details of the composition of γ -lines are “seen” by this selection of NN type events. E.g. the 2505.7 keV line (see Refs. 3 and 4) originating from summation of the subsequent 1173.2 and 1332.5 keV γ -lines from ^{60}Co naturally expected to be a *multiple site event* is *erased to 100%*. The neuronal net also reduced the 2016.7 keV line from ^{214}Bi which is as E0 transition also produced by two subsequent transitions (see Refs. 3 and 4), stronger than normal full energy (FE) γ -peaks.

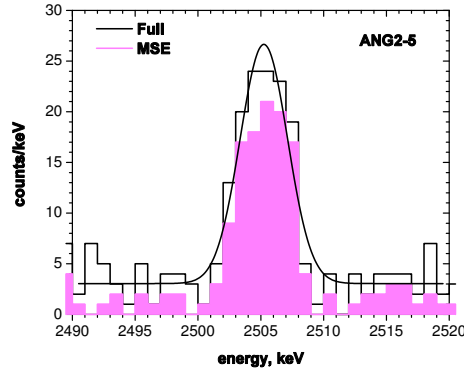


Fig. 6. Line from the full spectrum measured 1995–2003 (see also Figs. 15 and 16 of Ref. 4, and Fig. 3 of Ref. 3) and the pulse shape selected MSE spectrum on the basis of the neuronal net, (see Refs. 4, 16 and the text), for detectors 2, 3, 4, 5 in the energy region the 2505.7 keV γ -line.

cutting 1 or 2 mm from the detector borders. This is the *typical length* which could be passed by electrons emitted *on the surface* (e.g. conversion electrons). By such cut we should lose on the other hand almost *no* $\beta\beta$ -events, since for most $0\nu\beta\beta$ events produced in this border zone, not the full energy will be deposited in the detector and thus they will not show up in the line at $Q_{\beta\beta}$ (see also Refs. 6 and 7). According to Monte Carlo calculations about 4% of all $0\nu\beta\beta$ events produced homogeneously in the detector, are lost in this way in the border range (see Ref. 7).

The surrounding γ -lines are now practically completely erased, (compare to Fig. 19 of Ref. 4). This includes the structure at ~ 2030 keV. Only a tiny part is still seen of the 2053 keV ^{214}Bi line. The indication of a structure seen at ~ 2024 keV in the full spectrum (Figs. 17 and 18 of Ref. 4) which is still visible in Fig. 7 without border cut, seems to be a surface impurity vanishing with the 2 mm cut completely. What is remaining from the cut with the pulse library of Sec. 2, is a signal at $2038.4 \pm 0.3(\text{stat}) \pm 1.2(\text{syst})$ keV on a 4.0, 5.2, 6.0σ level for the 0, 1, 2 mm border cuts. The estimated systematical error comprises ballistic deficit, energy nonlinearity, etc. The result is *not* dependent on details of the applied library — it is obtained for the library in which the impurity distribution in the detectors is approximated by a constant distribution¹⁷ and *also* when the library is calculated using the realistic variation of the impurities along the direction of the detector axis, given by the manufacturers (see Table 2 in Ref. 17). The χ^2 values of the cuts change slightly, but the selected events remain (essentially) the same. From the cut with the neuronal net (NN — see below) we obtain (right column of Fig. 7) a signal at $2036.8 \pm 0.2(\text{stat}) \pm 1.2(\text{syst})$ keV on a 6.62, 7.23, 6.7σ level for the 0, 1, 2 mm border cut. The fits in Fig. 7 are made, conservatively assuming only one line in the energy window 2000–2060 keV, and assuming all other structures as constant background. If we allow lines at the positions of the known ^{214}Bi lines, the confidence levels in Fig. 7 become slightly larger. We would like to stress that we obtain the same *confidence* level for the signal *when we increase the energy window*

Table 1. All *global* neuronal net accepted events (plus one MSE event) in the energy region of 2035–2043 keV for detectors 2, 3, 4, 5.^{3,4} In the “Index” column: 0 – *global* neuronal net selection NN + HNR; 1 – Events selected by subclass of neuronal net method (NN); 2 – selected by low- χ^2 (see text) library cuts.

Det.	Run	Event	Type	Date	Energy	χ^2	R cm	Index		
								0	1	2
5	3357	2948	HNR	24.09.02	2034.39	0.33	3.45	+		+
3	3383	180	HNR	18.10.02	2035.14	0.77	1.84	+		
3	1627	172	HNR	15.05.99	2036.0	0.49	2.51	+		
3	749	295	NN	08.07.97	2036.04	1.68	2.7	+	+	
5	1067	421	NN	20.02.98	2036.31	0.98	2.65	+	+	
4	2613	47	NN	23.07.01	2036.37	1.72	1.99	+	+	
4	1762	97	HNR	28.08.99	2036.43	3.38	2.75	+		
3	3463	27	NN	07.01.03	2036.49	6.84	2.7	+	+	
5	2390	199	NN	27.01.01	2036.57	0.81	3.82	+	+	
2	2094	42	NR	20.05.00	2036.91	0.3	1.31			+
3	3385	354	HNR	21.10.02	2037.22	0.8	1.35	+		
5	1787	359	HNR	17.09.99	2037.22	0.31	1.91	+		+
5	2744	430	NN	21.11.01	2037.35	1.18	3.63	+	+	
3	108	112	NN	23.03.96	2037.58	0.81	2.45	+	+	
4	1271	251	HNR	01.08.98	2038.0	1.96	3.52	+		
3	2216	526	MSE	10.09.00	2038.3	0.38	1.1			+
4	1465	46	HNR	03.01.99	2038.33	5.9	2.75	+		
3	49	226	HNR	28.12.95	2038.53	0.26	2.27	+		+
4	1592	144	HNR	18.04.99	2038.57	0.53	1.99	+		+
2	735	131	HNR	28.06.97	2038.91	2.31	3	+		
4	2133	138	NR	24.06.00	2038.92	0.56	1.64			+
5	670	486	NN	09.05.97	2038.92	0.7	1.17	+	+	
3	3501	142	HNR	07.02.03	2038.97	0.74	2.7	+		
5	1036	73	HNR	26.01.98	2039.92	5.88	0.92	+		
3	1513	342	HNR	13.02.99	2039.93	0.55	2.27	+		
5	1650	206	HNR	03.06.99	2040.82	0.25	3.69	+		+
4	3449	74	HNR	22.12.02	2041.0	0.64	3.69	+		+
4	1378	490	HNR	27.10.98	2041.53	0.55	2.05	+		+
4	1125	296	HNR	05.04.98	2042.56	0.7	2.23	+		
4	3476	259	HNR	18.01.03	2042.75	0.78	1.35	+		
4	1833	74	HNR	22.10.99	2042.97	1.76	3.69	+		

considered. Figure 8 shows the NN selection for the range 2000–2100 keV. The fit yields a signal on a 6.4σ confidence level.

The events found by the zero range library and by the neuronal net subset (NN) (see below) are found to be *complementary* (see Table 1). We come back to this point below. Let us mention at this point, that the events selected by the neuronal net shown in Fig. 7 (right) are fitted by the zero range approximation library with slightly larger χ^2 (see Table 1), which partly may indicate larger sizes (see Refs. 17 and 18), or that the library is less optimized in the outer part of the detector.

The *sum* of the complementary spectra yields a line at $2037.5 \pm 0.5(\text{stat}) \pm 1.2(\text{syst})$ keV at a $5.2, 6.5, 6.8\sigma$ level (0, 1, 2 mm border cut), see Fig. 9.

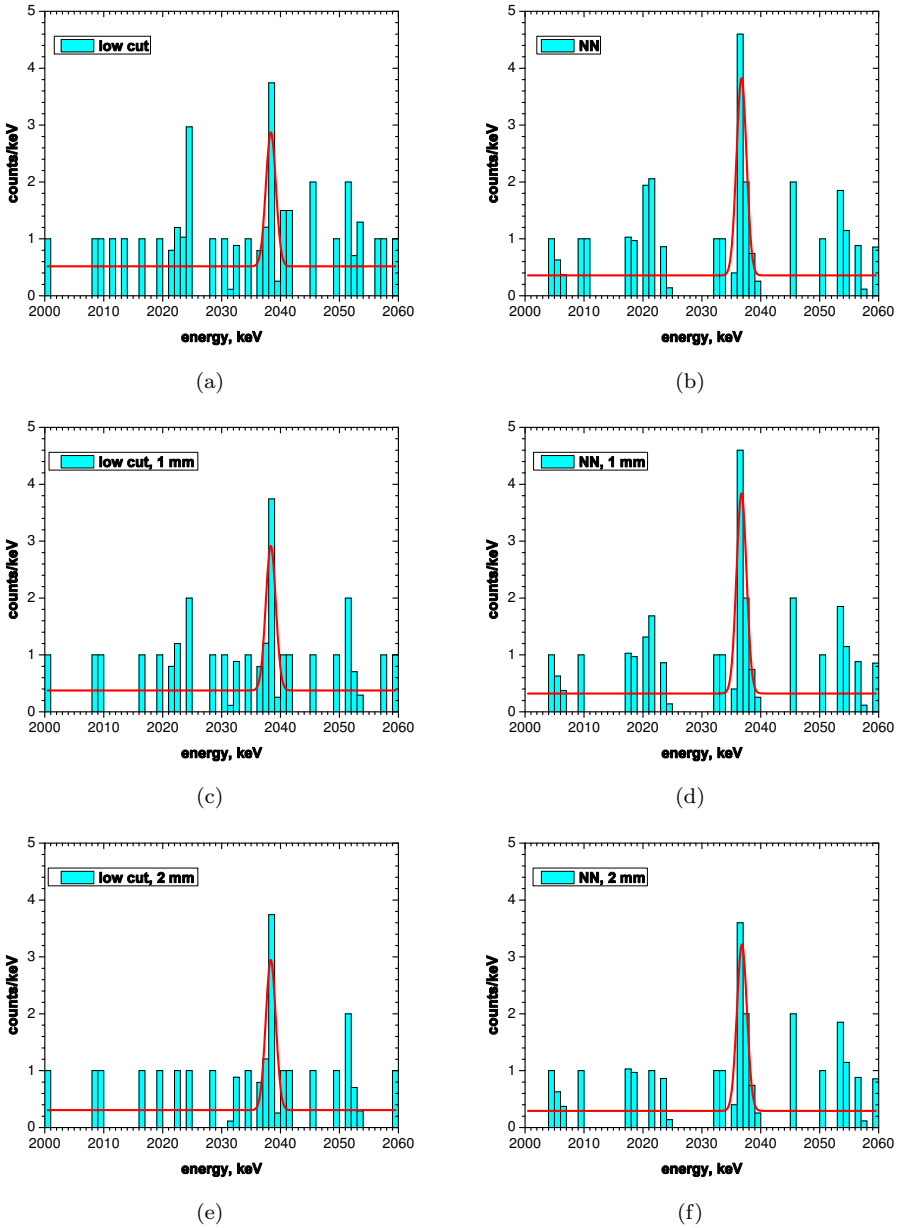


Fig. 7. Left column: The pulse shape selected spectrum after applying the zero range library (left column) with “small” cuts (see text) ((a), (c), (e)) measured with detectors 2, 3, 4, 5 from 1995 to 2003 in the energy range of 2000–2060 keV. The events in the full detector (a) and cutting boundary areas of 1(2) mm, (c) and (e) are shown. Signals are found near $Q_{\beta\beta}$ on a 4.0, 5.2 and 6.0 σ level (a), (c), (e), respectively: 5.03 ± 1.25 , 5.42 ± 1.04 and 5.63 ± 0.94 events. Right column: The pulse shape selected spectra (subsection NN by neuronal net, see Fig. 33 from Ref. 4 and text below) measured with detectors 2, 3, 4, 5 from 1995 to 2003 in the energy range of 2000–2060 keV. The events in the full detector (b) and cutting boundary areas of 1(2) mm, (d) and (f) are shown. The signals near $Q_{\beta\beta}$ are found on a 6.6, 7.2 and 6.7 σ confidence level ((b), (d), (f), respectively): 7.39 ± 1.12 , 7.50 ± 1.04 and 6.24 ± 0.93 events.

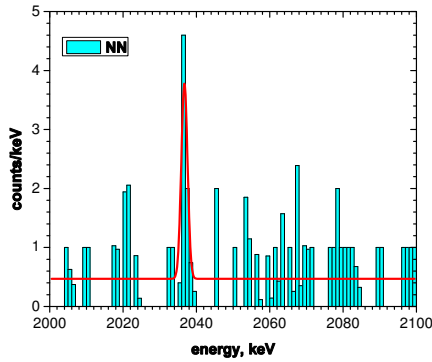


Fig. 8. The pulse shape selected spectrum (selected by neuronal net-NN) with detectors 2, 3, 4, 5 from 1995 to 2003 in the energy interval 2000–2100 keV (see Refs. 3 and 4). The signal at $Q_{\beta\beta}$ has a confidence level of 6.4σ (7.05 ± 1.11 events).

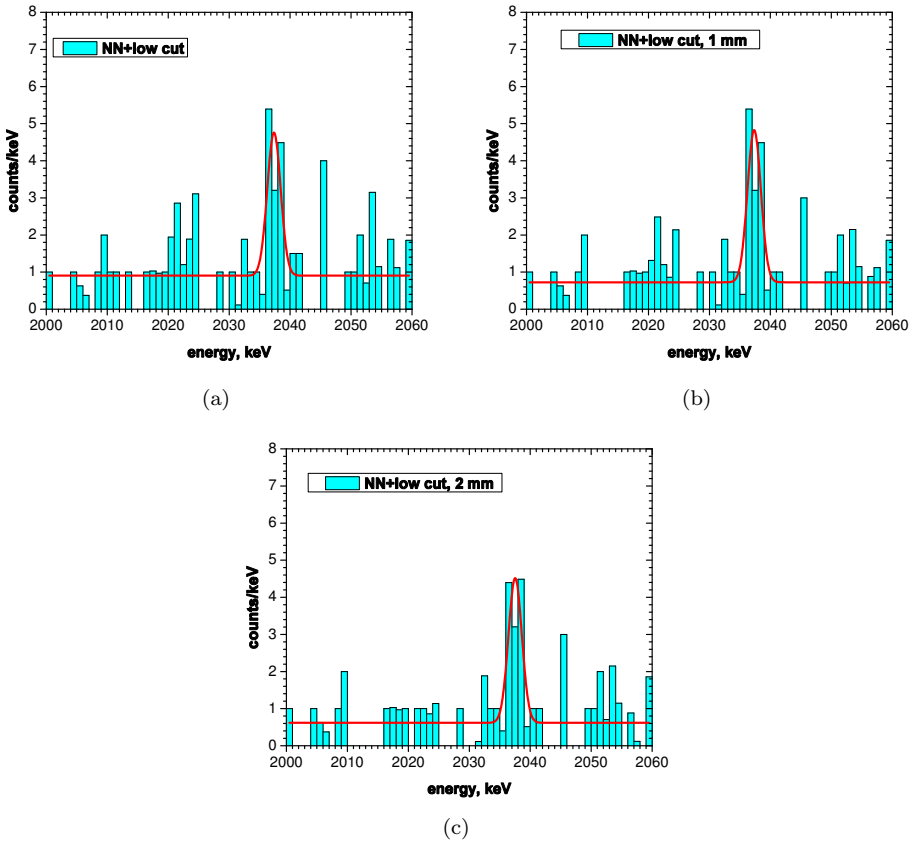


Fig. 9. The sum of the neuronally selected (NN) pulses and of the spectrum selected by the zero range library, measured with detectors 2, 3, 4, 5 from 1995 to 2003 in the energy range of (2000–2060) keV. Shown are the events observed in the full detector (a) and cutting the detector boundaries by 1, 2 mm. Signals near $Q_{\beta\beta}$ are found on a 5.2σ (10.64 ± 2.06 events), 6.5σ (11.32 ± 1.75 events) and 6.8σ (10.75 ± 1.58 events) confidence level (a, b, c, respectively).

How can we understand these findings? First, we note that practically all the events selected by the partial cuts, are contained in the global neuronal net selection given in Fig. 31 of Ref. 4 (see Table 1 and below). So *all* results given here and presented earlier^{3,4} are fully consistent. As can be seen from that figure, the *global* neuronal net based on the fit of events from the DE line (with a relaxed χ^2), is obviously *not selective enough* to reduce the gamma lines in the surroundings of $Q_{\beta\beta}$ strongly enough. There may be several reasons for that. Interestingly, however, *parts* of the full line at $Q_{\beta\beta}$ in Fig. 19 of Ref. 4 can be *projected out of the full data, practically without background*, by the *subset*, (which we call NN, see below) of the neuronal net given in Refs. 3 and 4 *and also* by the low- χ^2 cut of the pulse shape analysis (PSA) described in this paper. All events projected out by these two procedures are also selected by the full (“total”, see below) neuronal net of Refs. 3, 4 and 16 (see Table 1). They contain practically no multiple site events.

It may be necessary to go slightly more into detail to explain the notification used on the previous pages. We have discussed in Ref. 16 a neuronal method, (which we call N or “total” neuronal net here), calibrated with one line (the 1592 keV double escape line), and a second one (called R) calibrated with *two* lines (the 1592 keV double-escape line and the 2231.4 keV double escape line of the 3253.4 keV ^{60}Co line). The MSE library in the neuronal net is based on events of the 1621 keV ^{214}Bi total absorption peak. The “total” projection N by the neuronal method can be subdivided into events seen *only* by method N (called NN here), events seen by methods N and R (called NR), seen by methods N , R and the method (called H) developed in Ref. 14, see also Ref. 15, (called HNR). So the total projection by N can be written as sum of subprojections $N = \text{HNR} + \text{NN} + R + \text{NR} + \text{HN} + \text{HR}$. In Fig. 31 of Ref. 4 we show the projection obtained by $\text{HNR} + \text{NN}$ (what we call the “global” projection) which contains most of the N -events. No events of types R and HR are seen in the range 2036–2043 keV, and only one event of type HN, and 3 of type NR are seen.

From Table 1 we see that in addition to HNR events only *three* events are observed by the low cut of the PSA method — from which two are of NR type, i.e. which are *also* seen by the “total” neuronal net, and one is of MSE type.

The function of the low-cut PSA seems not to accept *those* HNR events, which *partly* form the background of the full line at $Q_{\beta\beta}$ in Fig. 19 of Ref. 4. Only one event is accepted by the low cut PSA, which is seen as MSE by the “global” neuronal net. This is consistent with the estimated efficiency of the neuronal method.¹⁶

In total, by the two projections, which show each a line near $Q_{\beta\beta}$ with almost no background, we find $9 + 8 = 17$ events in the energy range 2036–2043 keV according to Table 1. From these 11 to 12 events occur in the line from the fits shown in Figs. 7 and 9. This means we can identify the major part of the 19.6 ± 5.4 events, determined from the fit of the line in the full spectrum (Fig. 19 of Ref. 4), as $0\nu\beta\beta$ candidate events.

Considering only the NN events from Table 1 and the HNR events found by the low-cut PSA, these are in total 14 events, consistent with the 12.4 ± 3.7 events obtained by the neuronal net cut $\text{HNR} + \text{NN}$ in Fig. 31 of Ref. 4.

In conclusion, by the *two* projection procedures, the *major part* of the line near $Q_{\beta\beta}$ in the full spectrum is selected, while at the same time the surrounding γ -lines are *drastically reduced*. The selected events can be identified individually and are interpreted as events of $0\nu\beta\beta$ decay. Figures 10 and 11 show the pulses in the line at $Q_{\beta\beta}$ selected by the neuronal net (NN) and fits by the zero range approximation of Sec. 2. The radii at which the events are observed in the detector (determined by the zero range approximation of Sec. 2.3) are given in Table 1. The observed distribution as function of R is within the low statistics and the uncertainty of determination of R (see Fig. 2) consistent with that *expected* for a *homogeneous* source distribution.

Summarizing, with the two projections we suppress gamma lines almost *completely* and only a line at $Q_{\beta\beta}$ stands out. While the *global* or the *total* neuronal net used earlier^{3,4} sees *all* $0\nu\beta\beta$ events, but is not selective enough, to fully reduce the surrounding γ -lines, *sharper cuts* (low χ^2 cut introduced in this paper and neuronal

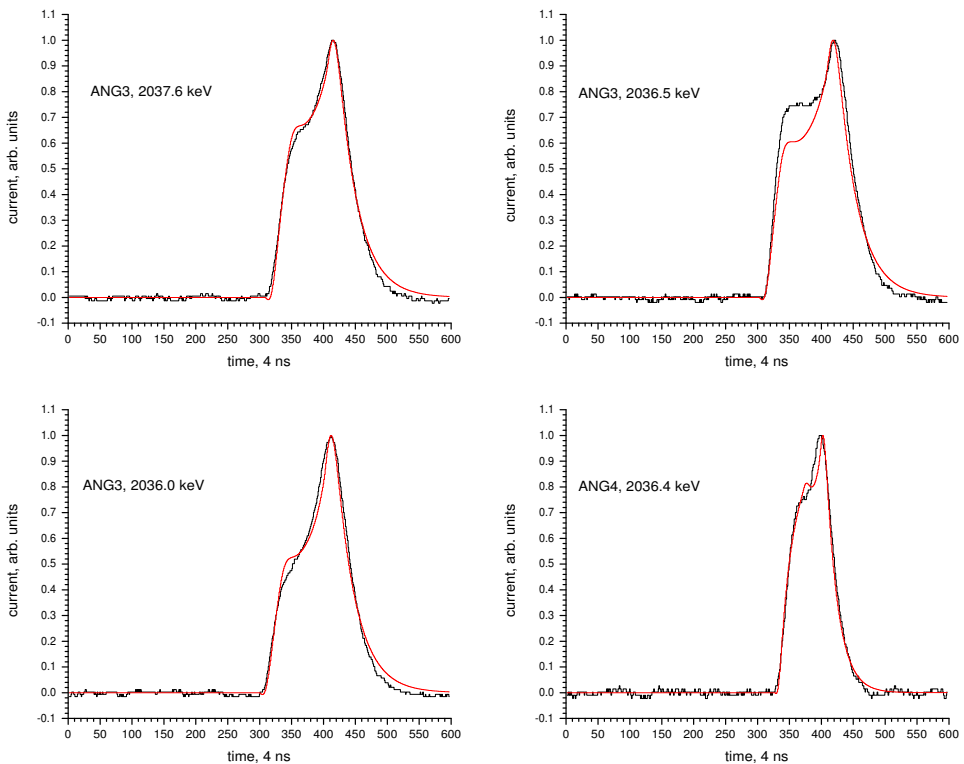


Fig. 10. Time structure of those events (black) measured in the Heidelberg–Moscow experiment in the energy region 2036–2042 keV by the four enriched ^{76}Ge detectors (ANG2, ANG3, ANG4, ANG5), during the period 1995–2003 selected by the neuronal net (NN selection, see text) as single-site events (see Table 1, and Fig. 9 of Ref. 3). The red lines show fits of the events by the zero range pulse shape approximation library, described here. The result is consistent with the former neuronal net analysis.

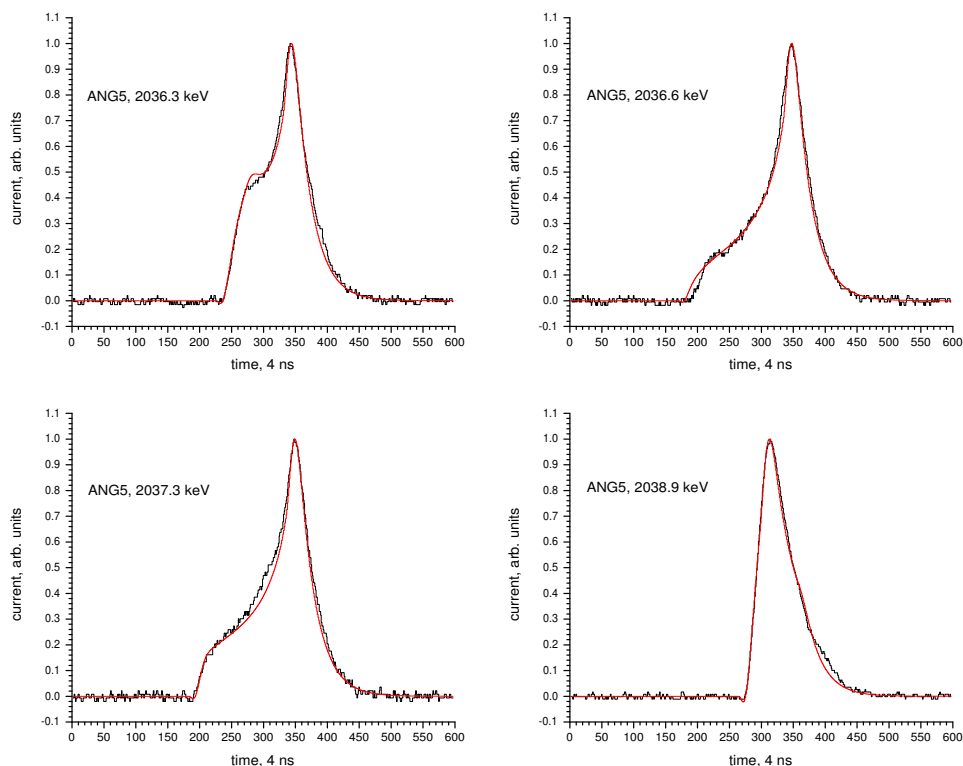


Fig. 10. (Continued)

subset NN already used in Ref. 3 and 4) *erase* the γ -lines and the $0\nu\beta\beta$ line stands out with practically *no background*.

The energy of the line observed (sum of NN and low- χ^2 cut), with $2037.5 \pm 0.5(\text{stat}) \pm 1.2(\text{syst})$ keV seems to be slightly below the “best” value reported for $^{35}Q_{\beta\beta}$ of 2039.006 ± 0.050 keV. Other measurements report $Q_{\beta\beta} = 2040.71 \pm 0.52$ keV,³² 2038.56 ± 0.32 keV³³ and 2038.668 ± 2.142 keV.³⁴

Part of this difference, and the *difference* in energy of the NN and low-cut lines in Fig. 7, seems to be due to the effect of the ballistic deficit (for definition see Ref. 20). Since in axial Ge detectors different radial location of events corresponds to large variation in the charge collection times and the latter may come close to the differentiation time of the electronic circuit, this leads if uncorrected, to a dependence of the measured energy from the radial location of the individual event and to a broadening of the observed line. We have investigated this effect (see Ref. 37). E.g. for detector ANG2 for single site events from the 2614 keV line from ^{228}Th a shift in the energy positions of around 7 channels (~ 2.4 keV) to lower energy is visible for the relatively slow pulses that start from the peripheral parts of the crystal with respect to the fastest pulses with initial radii of around 1.5 cm. For the other detectors this difference amounts to ~ 1 –1.6 keV. For energies

around $Q_{\beta\beta}$, due to the linear dependence of the energy shift on the event energy, a difference of ~ 1.8 keV is expected for detector ANG2 and of ~ 0.8 – 1.3 keV for the others (see Ref. 37).

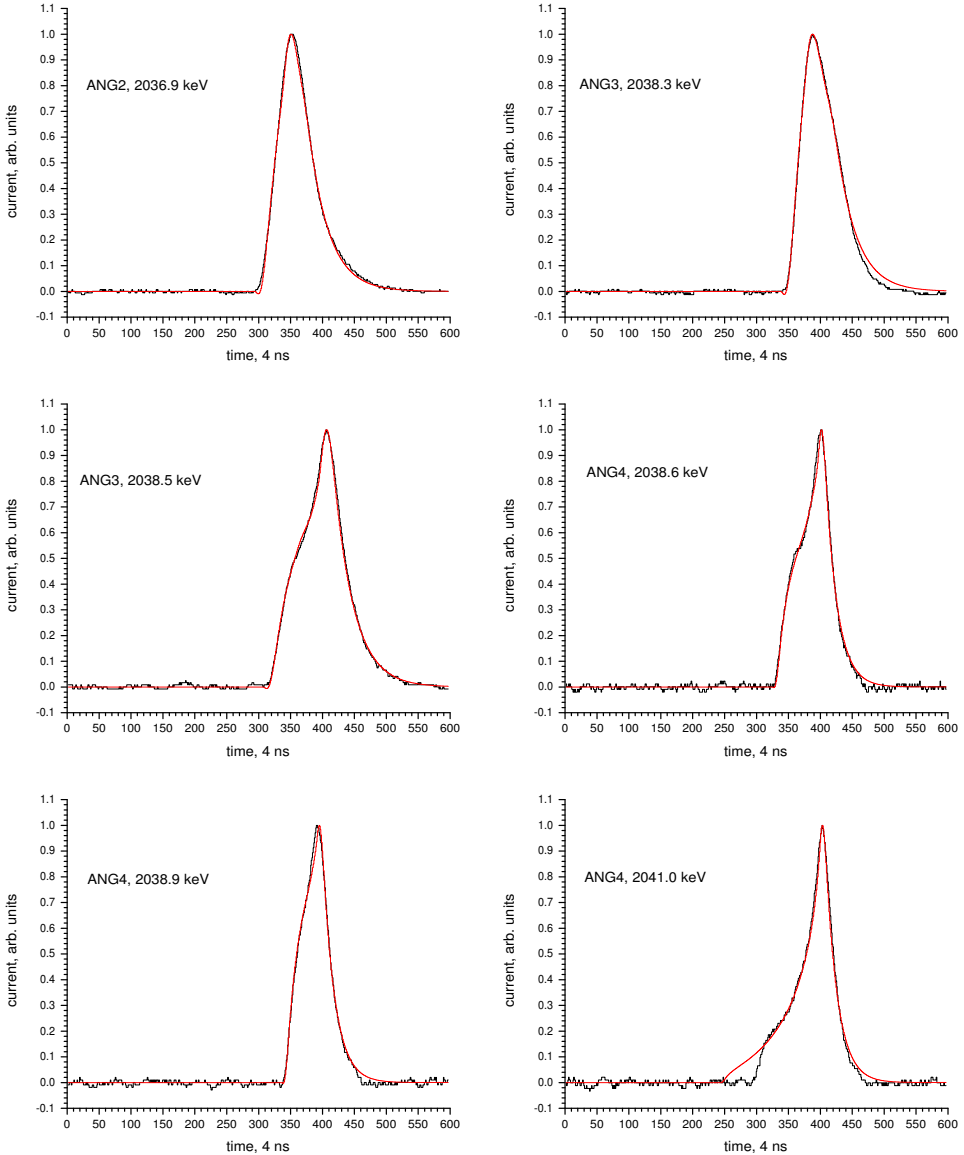


Fig. 11. Time structure of those events (black) measured in the Heidelberg–Moscow experiment in the energy region 2036–2042 keV by the four enriched ^{76}Ge detectors (ANG2, ANG3, ANG4, ANG5), which were identified, by the low-cut PSA method (Sec. 2) as single site events (see Table 1). The red lines show fits of the events by the zero range pulse shape approximation library, described in this paper and in Ref. 17.

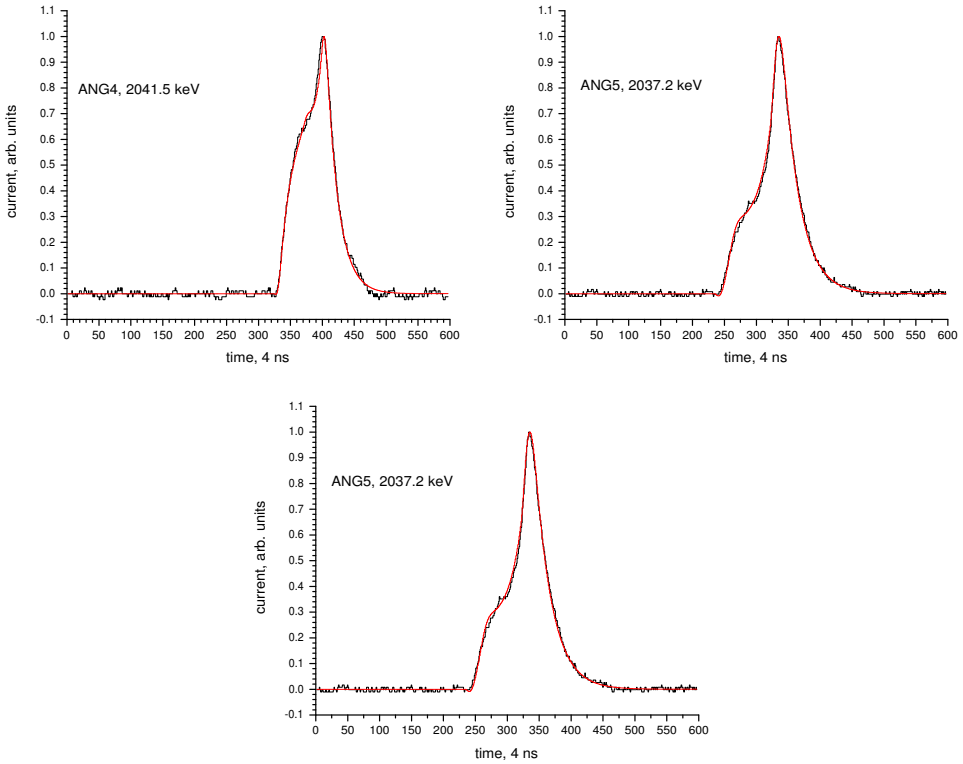


Fig. 11. (Continued)

4. Conclusion

We gave a description of the present evidence for the observation of $0\nu\beta\beta$ decay. Two completely different methods of pulse shape analysis have been used for the analysis of the data taken in the period 1995–2003. The first one uses a neuronal net for selection of $0\nu\beta\beta$ event candidates and has been described and applied already in Refs. 3, 4 and 16. Some details are given here for the first time. The second method developed recently uses a pulse shape library of point-like events calculated from the field distributions in the detectors as function of radius R and height Z of the detectors. These calculations have been described in Ref. 17, where it has also been shown microscopically, by Monte Carlo calculations, that the pulse shapes of such library events provide a good approximation of the pulse shapes of realistic $0\nu\beta\beta$ events and their spatial energy distribution.

By both methods, part of the line found at $Q_{\beta\beta}$ in the *full* spectrum is clearly *projected out with almost no background* from any surrounding γ rays, on a $\sim 6\sigma$ confidence level. It is found that *both sets of events are contained* in the selection of the *global* neuronal net used in Refs. 3 and 4. We consider this identification of events at $Q_{\beta\beta}$ and practically full suppression of the surrounding γ -background as

decisive proof for the observation of the $0\nu\beta\beta$ process. This proves that total lepton number is violated and, that the neutrino is a Majorana particle.

Starting from an intensity of the line in the pulse shape selected spectrum (sum of NN and low-cut spectra in Fig. 9) of 11 ± 1.8 events (i.e. close to that presented in Table 7 of Ref. 4 for the SSE events), leads to a half-life for $0\nu\beta\beta$ decay of $T_{1/2}^{0\nu} = (2.23_{-0.31}^{+0.44}) \times 10^{25}$ y. This agrees with the central value of the half-life determined from the *full* spectrum^{3,4} within a 1.7σ error of the latter.

From the half-life one can derive *some* information on the effective neutrino mass $\langle m \rangle$ and the right-handed weak current parameters $\langle \eta \rangle$, $\langle \lambda \rangle$. In general we *cannot* determine the individual contributions of $\langle m \rangle$, $\langle \eta \rangle$, $\langle \lambda \rangle$ from a single $\beta\beta$ experiment, but only *upper limits* (see Eq. (1)). Under the *assumption*, that only *one* of the terms contributes to the decay process, and ignoring potential other processes connected with SUSY theories, leptoquarks, compositeness, etc. (see Ref. 1), we find $\langle m \rangle = (0.32_{-0.03}^{+0.03})$ eV, or $\langle \eta \rangle = (3.05_{-0.25}^{+0.26}) \times 10^{-9}$, or $\langle \lambda \rangle = (6.92_{-0.56}^{+0.58}) \times 10^{-7}$, and thus can fix the effective neutrino mass. In that sense it is highly premature to compare, as often done, such number with numbers deduced from e.g. WMAP or other cosmological experiments, or to use it as a landmark for future tritium experiments - other than as an upper limit.

This fact also strongly relativates the popular and beloved efforts to calculate the nuclear matrix elements entering into Eq. (1). They are not very relevant at the moment for the extraction of fundamental physics. We use in derivation of the limits given above the nuclear matrix elements of Refs. 29 and 31. Since the corresponding matrix element for $2\nu\beta\beta$ decay underestimates this decay by $\sim 30\%$ (see Refs. 3 and 4) these calculations may also underestimate the $0\nu\beta\beta$ matrix element, and consequently the upper limit for the effective neutrino mass could be lower, down to ~ 0.22 eV.

It might be of some interest, to finally consider the potential of present and presently planned future experiments (1) to confirm the present result (2) to deliver additional information on the individual contributions of $\langle m \rangle$, $\langle \eta \rangle$, $\langle \lambda \rangle$, and others, to the $0\nu\beta\beta$ amplitude. For such discussion we refer to Refs. 6–8, 37 and 38.

References

1. H. V. Klapdor-Kleingrothaus, *60 Years of Double Beta Decay – From Nuclear Physics to Beyond the Standard Model* (World Scientific, 2001).
2. H. V. Klapdor-Kleingrothaus, *Int. J. Mod. Phys. D* **13**, 2107 (2004).
3. H. V. Klapdor-Kleingrothaus *et al.*, *Phys. Lett. B* **586**, 198 (2004).
4. H. V. Klapdor-Kleingrothaus *et al.*, *Nucl. Instrum. Meth. A* **522**, 371 (2004).
5. H. V. Klapdor-Kleingrothaus *et al.*, *Mod. Phys. Lett. A* **16**, 2409 (2001); *Found. Phys.* **31**, 1181 (2002) [Erratum, *ibid.* **33**, 678 (2003)].
6. H. V. Klapdor-Kleingrothaus, I. V. Krivosheina and I. V. Titkova, *Phys. Lett. B* **632**, 623 (2006).
7. H. V. Klapdor-Kleingrothaus, I. V. Krivosheina and I. V. Titkova, *Phys. Rev. D* **73**, 013010 (2006).

8. H. V. Klapdor-Kleingrothaus, I. V. Krivosheina and I. V. Titkova, *Int. J. Mod. Phys. A* **21**, 1159 (2006).
9. H. V. Klapdor-Kleingrothaus, in *Proc. of Int. Conf. on Neutrinos and Implications for Physics Beyond the Standard Model*, Stony Brook, USA, 11–13 October, 2002, ed. R. Shrock (World Scientific, 2003), pp. 367–382; in *Proc. of Intern. Conf. on Beyond the Desert 2003, BEYOND03*, Tegernsee, Germany, 9–14 June, 2003, ed. H.V. Klapdor-Kleingrothaus (Springer, Heidelberg 2004), pp. 307–364.
10. H. V. Klapdor-Kleingrothaus, in *Proc. Int. Conf. NEUTRINO 2004*, 14–19 June 2004, Paris, France, *Nucl. Phys. B (Proc. Suppl.)* **143**, 229 (2005).
11. H. V. Klapdor-Kleingrothaus, in *Proc. Int. Workshop on Neutrino Oscillations NOW2004*, 11–17 September 2004, Otranto, Italy, eds. G. Fogli *et al.*, *Nucl. Phys. B (Proc. Suppl.)* **145**, 219 (2005).
12. H. V. Klapdor-Kleingrothaus, in *Proc. of Int. Conf. on Neutrino Telescopes*, February 2005, Venice, Italy, ed. M. Baldo-Ceolin, p. 215, hep-ph/0512263.
13. H. V. Klapdor, Proposal, Internal Report, MPI-1987-V17, September 1987.
14. J. Hellmig and H. V. Klapdor-Kleingrothaus, *Nucl. Instrum. Meth. A* **455**, 638 (2000).
15. J. Hellmig, F. Petry and H. V. Klapdor-Kleingrothaus, Patent DE19721323A.
16. B. Majorovits and H. V. Klapdor-Kleingrothaus, *Eur. Phys. J. A* **6**, 463 (1999).
17. H. V. Klapdor-Kleingrothaus, I. V. Krivosheina, V. Mironov and I. V. Titkova, *Phys. Lett. B* **636**, 235 (2006).
18. H. V. Klapdor-Kleingrothaus, I. V. Krivosheina and I. V. Titkova, *Int. J. Mod. Phys. A* **21**, 1 (2006).
19. <http://laacg1.lanl.gov/laacg/>; K. Halbach and R. F. Holsinger, *Part. Acc.* **7**, 213 (1976).
20. G. F. Knoll, *Radiation Detection and Measurement*, 2nd edn. (John Wiley & Sons, 1989); K. Siegbahn, *Alpha-, beta- and Gamma-Ray Spectroscopy* (North-Holland, 1974), Vol. 1 and 2.
21. K. Vetter *et al.*, *Nucl. Instrum. Meth. A* **452**, 105 (2000).
22. K. Vetter *et al.*, *Nucl. Instrum. Meth. A* **452**, 223 (2000).
23. Th. Kröll and D. Bazzacco, *Nucl. Instrum. Meth. A* **463**, 227 (2001).
24. L. Milechina and B. Cederwall, *Nucl. Instrum. Meth. A* **550**, 278 (2005).
25. C. E. Lehner *et al.*, in *Proc. of Electronics Engineers Nucl. Science Symp.*, San Diego, CA, Nov. 5–10, 2001.
26. T. W. Raudorf, private communication, 2006.
27. T. W. Raudorf, M. O. Bedwell and T. J. Paulus, *IEE Trans. Nucl. Sci.* **NS-29**, 764 (1982).
28. Ch. Dörr and H. V. Klapdor-Kleingrothaus, *Nucl. Instrum. Meth. A* **513**, 596 (2003).
29. A. Staudt, K. Muto and H. V. Klapdor-Kleingrothaus, *Eur. Lett.* **13**, 31 (1990).
30. K. Muto and H. V. Klapdor, in *Neutrinos*, ed. H. V. Klapdor (Springer, 1988), pp. 183–238.
31. K. Muto, E. Bender and H. V. Klapdor, *Z. Phys. A – Atomic Nucl.* **334**, 187; 177 (1989).
32. R. J. Ellis *et al.*, *Nucl. Phys. A* **435**, 34 (1985).
33. J. G. Hykawy *et al.*, *Phys. Rev. Lett.* **67**, 1708 (1991).
34. G. Audi and A. H. Wapstra, *Nucl. Phys. A* **595**, 409 (1995).
35. G. Douysset *et al.*, *Phys. Rev. Lett.* **86**, 4259 (2001); I. Bergström *et al.*, in *Proc. of Int. Conf. on Particle Physics Beyond the Standard Model, BEYOND'02*, Oulu, Finland June 2002, IOP, 2003, ed. H. V. Klapdor-Kleingrothaus, in *BEYOND 2003*, Castle Ringberg, Germany, 10–14 June, 2003, ed. H. V. Klapdor-Kleingrothaus (Springer, 2003).

36. K. Ya. Gromov *et al.*, *J. Part Nucl. Lett.* **3**, 30 (2006).
37. H. V. Klapdor-Kleingrothaus *et al.*, to be published.
38. H. V. Klapdor-Kleingrothaus, in *Proc. Int. Conf. SNOW2006*, May 2006, Stockholm, Sweden, *Phys. Scripta* (2006).
39. H. V. Klapdor-Kleingrothaus *et al.*, *Phys. Lett. B* **578**, 54 (2004); *Nucl. Instrum. Meth. A* **511**, 335 (2003); H. V. Klapdor-Kleingrothaus, hep-ph/0205228.